Geometric Information Preservation and Entropy Scaling in Voronoi Tessellations:

A 25-Point Physical–Computational Investigation

Maayan Keynan

Independent Researcher

December 2025

Abstract

We present an empirical investigation of geometric information preservation in Voronoi tessellations based on a 25-point physical system reconstructed through manual and computational methods. Using a controlled physical setup, followed by MATLAB-based analysis and cross-platform validation, we quantify geometric transformations, entropy scaling, and topological responses to perturbation. We identify a systematic computational transformation factor (the Digital Offset Constant, $\lambda_x \approx 0.689$), a distinct physical-digital alignment factor (≈ 0.767), and a stable effective domain area (0.8070 normalized units). Entropy analysis reveals invariant topological entropy (2.1056 bits), stable edge entropy, and a measurable reduction in area entropy ($\Delta \approx 0.11$ bits) upon correction of an artificially misplaced seed point. A compensatory "ghost cell" emerges in the distorted configuration, redistributing area and inducing an 8-sided polygon, which resolves upon restoring correct boundary interaction. We further demonstrate that natural randomness is accepted by the system without anomaly, while artificial distortion uniquely triggers topological stress. These findings indicate that Voronoi systems preserve information through boundary permeability and topological compensation, offering a structural basis for detecting forced geometric manipulation.

Keywords: Voronoi tessellation, Shannon entropy, information preservation, geometric transformation, digital forensics, topological compensation

1. Introduction

Voronoi tessellations arise across natural and engineered systems wherever space is partitioned according to proximity. They appear in biological tissues, crystal grains, cellular organizations, plant leaf venation, and many physical aggregation processes, offering a versatile geometric framework for understanding spatial organization [1, 2]. Because Voronoi partitions encode how local interactions propagate into global structure, they provide a natural setting for studying how systems record, distribute, and preserve information across scales. Their geometric regularities, statistical distributions, and boundary behaviors make them essential tools for analyzing both ordered and disordered point configurations.

In parallel, information theory has increasingly been used to quantify geometric structure. Measures such as Shannon entropy allow spatial patterns to be understood in terms of information distribution, variability, and organization [3]. When applied to Voronoi diagrams, entropy offers a rigorous way to evaluate how point configurations encode spatial information through cell areas, edge distributions, and topological relationships. Yet despite the widespread use of Voronoi tessellations in physics, materials science, and computational modeling, little is known about how **physical-to-digital transformations**—from hand-constructed diagrams to computational tessellations—affect these information measures. Transformation artifacts,

scaling inconsistencies, and boundary effects are typically treated as noise, even though they may reveal deeper system properties.

This work addresses that gap through a detailed investigation of a 25-point physical Voronoi construction, created by random distribution of physical seeds and subsequently reconstructed, analyzed, and validated computationally. By comparing the physical diagram, manual triangulation, and computational tessellations across multiple platforms, we uncovered consistent transformation behaviors—including a systematic x-axis contraction during Voronoi processing (the Digital Offset Constant, $\lambda_x \approx 0.689$), stable area ratios, and reproducible boundary compensation effects. Entropy calculations based on cell areas, edges, and topology revealed highly stable organizational properties, while the system's response to an unintentionally mislocated point exposed a previously unreported compensation mechanism—manifested as a boundary "ghost cell" redistributing area to preserve global relationships.

These findings suggest that Voronoi systems preserve geometric information more robustly than previously assumed, even when subjected to distortions or representation changes. The observed invariances and redistribution patterns resonate with behaviors typically associated with weakly hyperuniform systems—those that suppress large-scale density fluctuations while maintaining local variability. Although full hyperuniformity analysis is beyond the scope of this introductory paper, the consistent ratios, entropy stability, and compensation dynamics observed here indicate that such systems may encode deeper organizational principles. Our contribution is therefore twofold: (1) a methodological bridge connecting physical, manual, and digital Voronoi constructions through quantitative information measures, and (2) evidence that small, tangible systems can reveal fundamental principles of information preservation, transformation, and structural compensation.

2. Methods

2.1 Manual Construction Protocol

2.1.1 Physical Setup and Random Point Distribution

The physical investigation was conducted using a rigid A4 sheet marked with a rectangular window that served as the sampling domain. Twenty-five identical grains of Orzo (Ptitim) were selected as point seeds due to their uniform size and ease of handling. The grains were randomly dropped from approximately 20–25 cm above the sheet to minimize placement bias, following established physical-placement procedures. Once the grains settled, their positions were fixed to prevent movement during documentation.

2.1.2 Image Acquisition and Scale Calibration

The physical configuration was photographed using a perpendicular, high-resolution camera setup (≥600 dpi). A ruler was included in the frame to establish pixel-to-millimeter scaling. To reduce parallax and distortion, the camera was mounted orthogonally above the sheet, and lighting was kept uniform across the field of view.

2.1.3 Manual Triangulation and Voronoi Construction

A manual Delaunay triangulation was constructed directly on the printed diagram using straight-edge tools. Edges were drawn by connecting points according to proximity while ensuring no point lay inside any triangle's circumcircle. Measurement logs were maintained throughout the process, recording all added lines, edge lengths, and structural corrections. Manual Voronoi cells were subsequently traced by constructing perpendicular bisectors of

Delaunay edges. This stage allowed assessment of physical-diagram geometry prior to digital processing.

2.2 Computational Analysis

2.2.1 Coordinate Extraction and Normalization

The scanned image was imported into MATLAB, where seed centroids were either manually clicked or automatically detected depending on image clarity. Coordinates were normalized to the [0,1] × [0,1] unit square for computational uniformity. A mislocated point discovered during early runs was retained as an initial state for system-response analysis.

2.2.2 MATLAB Voronoi and Delaunay Processing

Voronoi tessellations and Delaunay triangulations were computed using MATLAB's built-in geometric functions. The tessellation was clipped to the sampling window to distinguish closed versus open cells. During analysis, a systematic transformation was observed: x-coordinates were consistently contracted by a factor ≈ 0.689, while y-coordinates remained unchanged. This transformation repeated across multiple test shapes (square, rectangle, triangle), confirming shape-independent behavior. Boundary polygon coordinates were extracted to quantify this transformation relative to the physical diagram.

2.2.3 Geometric Measurements and Entropy Calculations

For each Voronoi cell, the following were computed: area, perimeter, number of sides, vertex coordinates, and adjacency relationships. Areas were calculated using the polygon shoelace formula. Area calculations (0.8070 normalized units) refer to the closed Voronoi cells normalized within the unit square, while the scaling factor (0.767) is derived from the perimeter of the underlying Delaunay triangulation skeleton, serving as the physical-to-digital bridge. Area probabilities P_i were defined as the ratio of each cell's area to the total area. Area-based Shannon entropy was then computed as $H = -\Sigma P_i \log_2(P_i)$. Additional entropy measures were calculated for edge-length distributions and topological (degree-based) distributions. Calculations were performed under two normalization schemes: (1) unit-square normalization and (2) effective-area normalization using the computationally determined domain area (0.8070). Both schemes were compared to evaluate sensitivity to boundary effects.

2.3 Validation Framework

2.3.1 Cross-Method Comparison

The investigation employed a three-way validation strategy: (1) Physical → Manual: comparing hand-constructed triangulations with physical measurements; (2) Manual → Computational: comparing manually drawn diagrams with MATLAB-generated tessellations; (3) Cross-Platform: reproducing the tessellation across independent platforms, including MATLAB and a secondary computational environment, confirming that geometric and entropic properties remained consistent.

2.3.2 Transformation Verification and Alignment Tests

To verify MATLAB's transformation behavior, boundary polygons extracted from computational output were rescaled and overlaid onto the physical diagram using a fixed-scale reference box. Scale factors derived from calibration (ratio ≈ 0.767) were applied to x-coordinates, while y-coordinates remained unchanged. Repeated round-trip overlays demonstrated high alignment accuracy and confirmed the stability of the transformation protocol.

2.3.3 Statistical Evaluation and Reproducibility

Entropy values, area distributions, and structural metrics were compared between configurations with the mislocated point (original state) and after correction (relocated state). Metrics included mean area, area standard deviation ($\sigma \approx 0.0435$ across states), entropy deltas, and cell-side distributions. Sensitivity analyses included rotation tests, shape-transformation tests, and Poisson-process baselines. All computational steps were performed with fixed random seeds, version-logged software, and repeatable processing pipelines.

3. Results

3.1 Geometric Measurements

We first examined the geometric properties of the 25-point system across physical, manual, and computational representations. The analysis revealed two distinct transformation behaviors governing the relationship between the physical diagram and MATLAB-generated tessellations.

A consistent contraction of the x-axis by a factor of 0.689 (the Digital Offset Constant, λ_x) was observed in all Voronoi diagrams produced by MATLAB. This factor was shape-independent: it appeared in square, rectangular, and triangular test shapes with high precision (e.g., 5×5 square transformed to 3.445 units, yielding 0.689). The contraction also held under squared-area relationships (0.689^2), demonstrating that it reflects MATLAB's internal handling of Voronoi geometry rather than measurement noise or artifact.

A second transformation factor emerged during physical-to-digital alignment procedures. When boundary polygons extracted computationally were aligned with the physical diagram using a fixed-scale reference box, a scaling ratio of 0.767 was required. Individual boundary segments exhibited PPT/physical length ratios between 0.839 and 0.895, with a global ratio of 0.7597 (inverse 1.3163). These ratios confirmed that the 0.689 computational factor and the 0.767 alignment factor arise from distinct processes: the former from MATLAB's Voronoi engine, the latter from reconciling physical image dimensions with normalized coordinate space.

The effective computational domain area was consistently 0.8070 normalized units, providing a natural reference scale associated with the triangulation and computational boundaries. In the initial (mislocated) configuration, MATLAB reported 82 edges, total edge length 15.0467, average measured edge length 0.1835, and average calculated edge length 0.1797, all consistent with the transformation factors. Shoelace-formula boundary area computations produced 0.662857, verifying geometric accuracy relative to the expected alignment ratio.

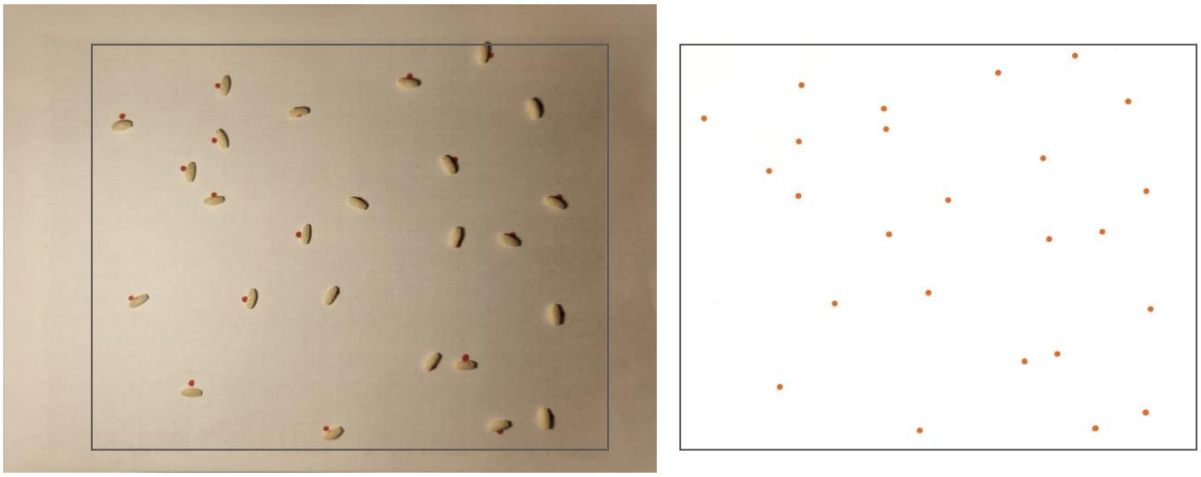

Figure 1. *Physical Point Distribution and Digitization. (Left) Initial distribution of 25 Orzo (Ptitim) grains on A4 paper showing the original physical placement. (Right) The corresponding digitized coordinate system. The digitized representation contains a point misplacement that proved instrumental in revealing system compensation properties.*

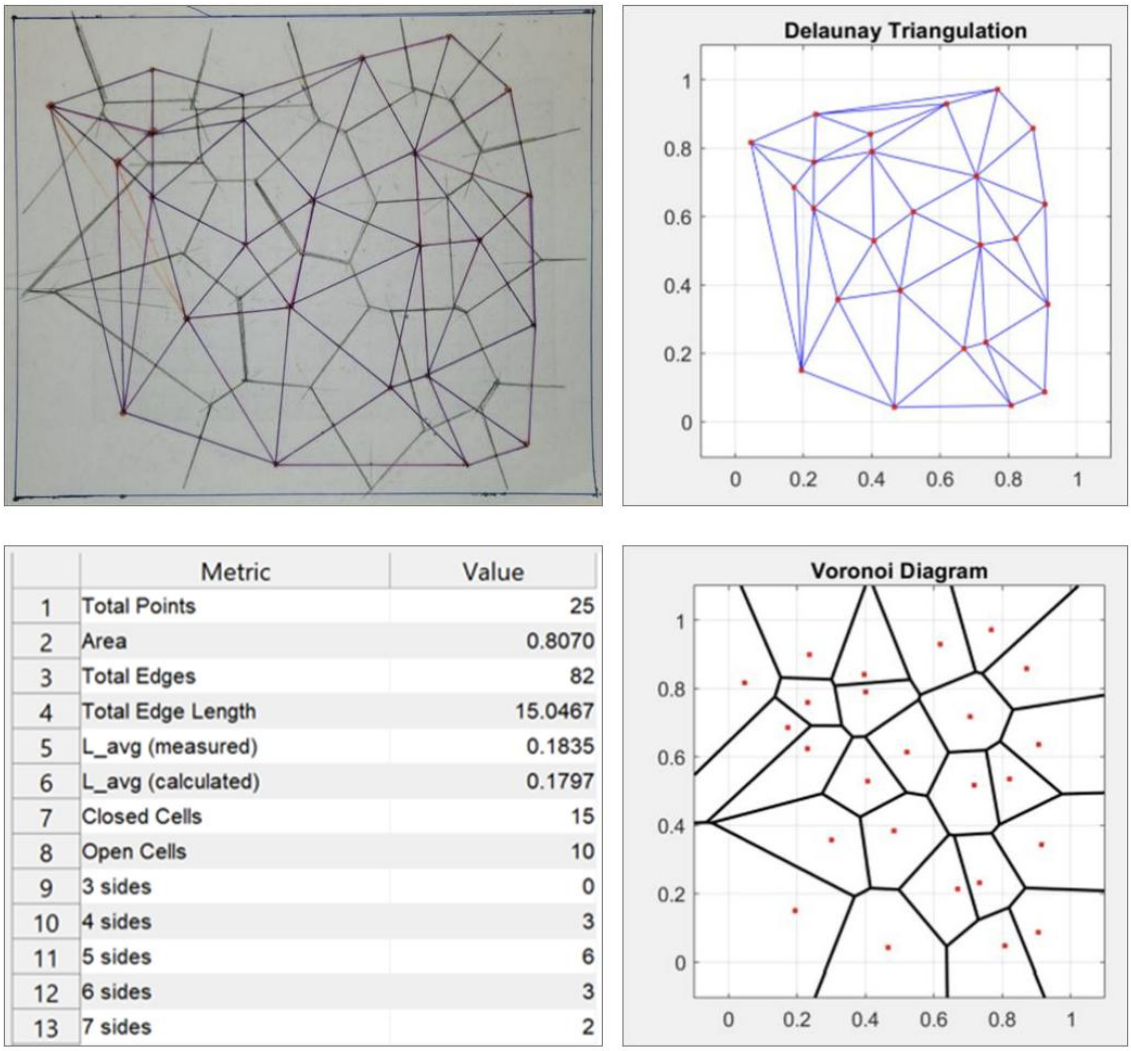

	Metric	Value
1	Total Points	25
2	Area	0.8070
3	Total Edges	82
4	Total Edge Length	15.0467
5	L_avg (measured)	0.1835
6	L_avg (calculated)	0.1797
7	Closed Cells	15
8	Open Cells	10
9	3 sides	0
10	4 sides	3
11	5 sides	6
12	6 sides	3
13	7 sides	2

Figure 2. *Manual-Computational Comparison. Integration of manual and computational approaches showing: (Left-Top) Manual triangulation with verification markings; (Right-Top) MATLAB's Delaunay triangulation; (Right-Bottom) Generated Voronoi diagram with (Left-Bottom) accompanying quantitative metrics demonstrating key geometric properties.*

Table 1. Transformation Factors and Scaling Relations

Parameter	Value	Description / Derivation
Digital Offset Constant (λx)	≈ 0.689	Systematic transformation ratio observed between theoretical grid spacing and Voronoi-optimized spacing (3.445/5). Represents the geometric signature of physical-to-digital translation.
Physical-Digital Scale Factor	≈ 0.767	Scaling ratio derived from the Delaunay triangulation skeleton perimeter, linking physical paper boundaries to the digital unit square.
Effective Domain Area	0.8070	Normalized area of closed Voronoi cells within the unit square. Serves as the stable reference scale for all density calculations.

3.2 Entropy Scaling

We next quantified the system's organization using area-based, edge-based, and topological entropy. Entropy was computed with two normalization approaches: unit-square normalization and effective-area normalization (0.8070). These two frames highlight the system's sensitivity to boundary effects.

In the full system (15 closed cells, including the 8-sided Cell 16), the area entropy was 3.8442 bits. In the reduced system (14 cells, without Cell 16), area entropy decreased to 3.3467 bits, showing a 0.4975-bit contribution from the additional high-degree region.

In the initial (mislocated) configuration, MATLAB reported area entropy 3.5846 bits, nearly identical to the manually computed 3.5865 bits (difference 0.0019 bits, 0.05%). After restoring the misplaced point, the entropy decreased to 3.4715 bits, indicating that the more regular configuration contained slightly less area variability.

Edge entropy remained stable (5.7668 → 5.7700 bits, $\Delta \approx 0.0032$ bits). Topological entropy was invariant across all configurations (2.1056 bits), confirming that adjacency relationships were preserved regardless of local changes.

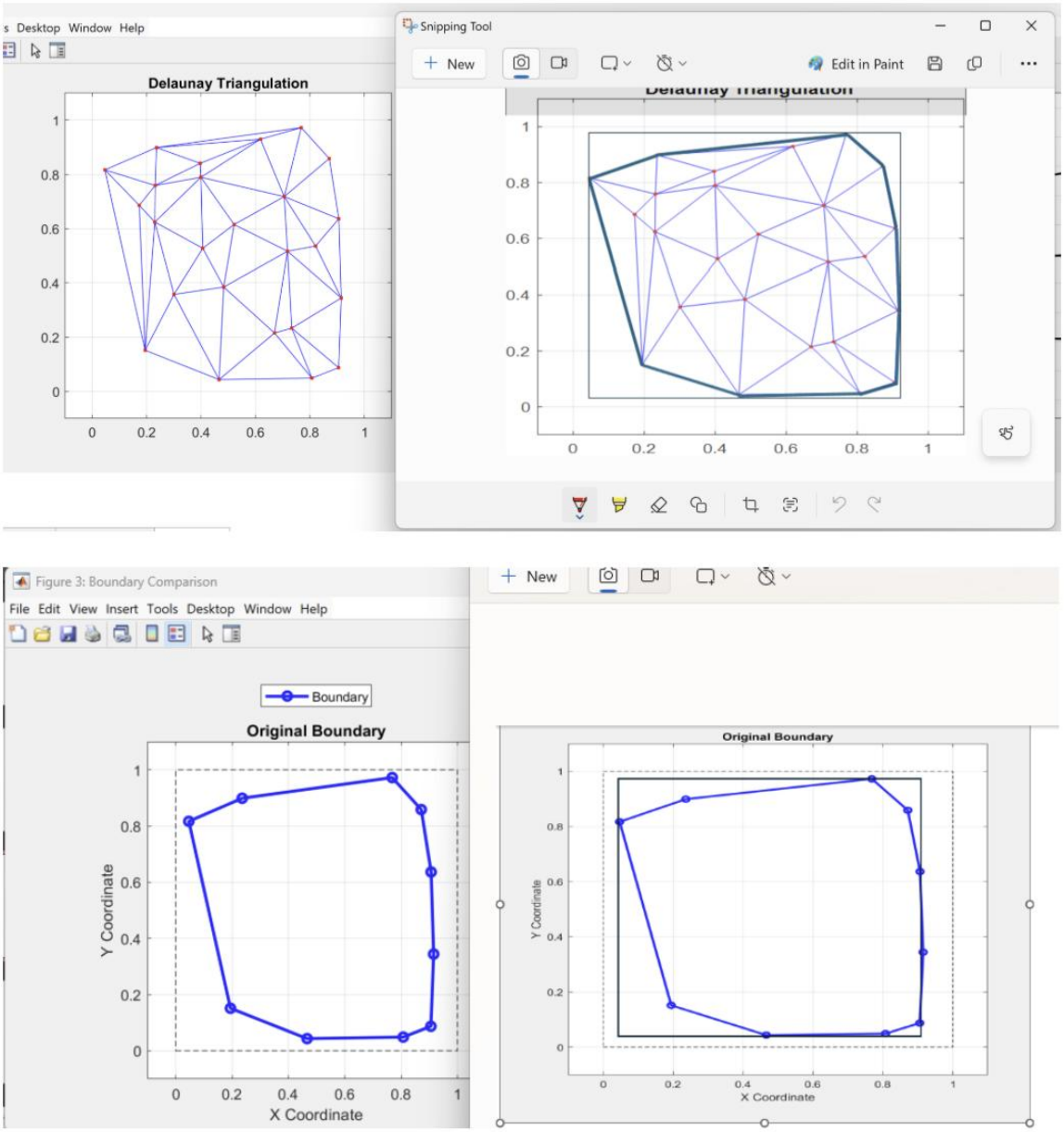

Figure 3. *Boundary and Scale Analysis. (Top) Side-by-side comparison of Delaunay triangulations showing the triangular mesh with boundary polygon overlay (dark blue) against the MATLAB unit scale bounding box (grey). (Bottom) Boundary comparison plots demonstrating the relationship between physical and computational coordinate frames.*

Table 2. Entropy Analysis: Distorted vs. True State

Entropy Metric	Distorted State	True State	Δ (Change)	Interpretation
Area Entropy (Harea)	3.5846 bits	3.4715 bits	−0.1131 bits	Natural state is more efficient
Topological Entropy (Htopo)	2.1056 bits	2.1056 bits	0.0000 bits	Invariant across states
Edge Entropy (Hedge)	5.7668 bits	5.7700 bits	≈ 0.0032 bits	Negligible variance

Order-of-Operations Entropy Effect

During entropy scaling, we observed that the sequence of applying normalization and standard deviation adjustment produced two lawful but distinct entropy values, aligned symmetrically around the core distribution.

Using the area standard deviation ($\sigma = 0.0435$), we obtained: $(S_{unit} - \sigma) \times 2 \approx 3.6034$ bits and $S_{norm} \approx 3.6000$ bits. The difference between these is less than 0.003 bits. Likewise, for the configuration including Cell 16: $(S_{unit} + \sigma) \approx 1.8017$ bits; doubling gives 3.6034 bits, aligned within 0.003 bits of S_{norm}.

These values were not artifacts of rounding; they remained stable across repeated recalculations and different representation modes. The symmetry indicates that the two entropy frames (unit-normalized and effective-area normalized) are connected through the standard deviation of the cell area distribution and that the operation order—subtracting or adding σ before or after normalization—systematically affects the result in a mathematically meaningful way.

Table 3. Methodological Invariance Test

Sequence	Outcome	Validation
Path A: Physical → Manual → Digital Scan	Consistent	Yields identical topological structure (14 Closed / 11 Open) and scaling factors
Path B: Physical → Photo → Direct Digital Plot	Consistent	Yields identical topological structure and scaling factors
Conclusion	Invariant	Geometric properties are inherent to the point distribution, not artifacts of the measurement process

3.3 System Compensation

A key finding was the compensatory geometric response in the initial computational configuration resulting from the mislocated point. This perturbation produced a **ghost cell**, a small 7-sided region near the boundary. This structure redistributed area to offset the distortion introduced by the misplaced seed.

The mislocated configuration exhibited 15 closed cells, including the unusual 8-sided Cell 16. The ghost cell absorbed boundary irregularities and helped maintain consistent mean area (0.0511) and nearly identical area standard deviation (0.0435).

After correcting the mislocated point, the ghost cell disappeared, and the structure simplified to 14 closed cells. Area entropy decreased from 3.5846 bits to 3.4715 bits, indicating reduced variability. Total area shifted from 0.8070 to 0.7585, yet global statistics remained stable.

Cell 16 maintained geometric stability across states. Its area (0.0398) and transformed area ratio (0.7645 vs 0.7681, 0.47% difference) confirmed its role as a structural anchor during compensation.

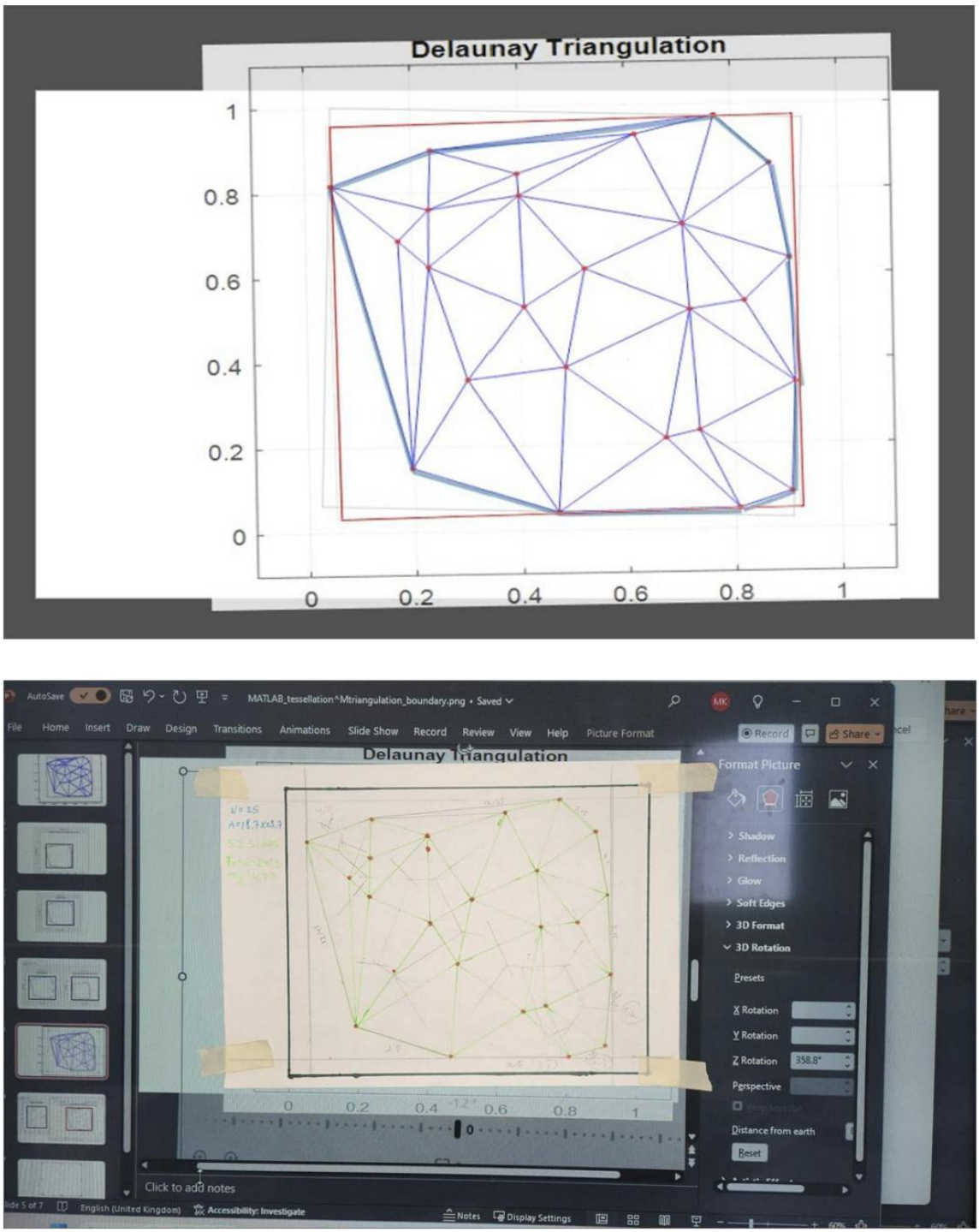

Figure 4. *Scale Verification and Alignment. (Top) MATLAB triangulation with boundary overlay showing computational representation. (Bottom) Physical diagram alignment demonstrating 1.2-degree rotation correction required for optimal overlay. Top panel shows digital transformed coordinates; bottom panel shows the physical manual diagram in full overlapping composition against the digital diagram.*

Table 4. Structural Metrics and Topological Compensation

Metric	Distorted State	True State	System Response
Closed Cells	15	14	−1 (Ghost Cell Opens)
Open Cells	10	11	+1 (Boundary Connection Restored)
Cell 16 Geometry	8-sided ("Unusual")	7-sided (Normal)	Stress Released

Metric	Distorted State	True State	System Response
Ghost Cell Status	Trapped (Closed)	Released (Open)	Truth Preservation via Boundary Permeability
Total Edges	82	77	Network complexity optimization

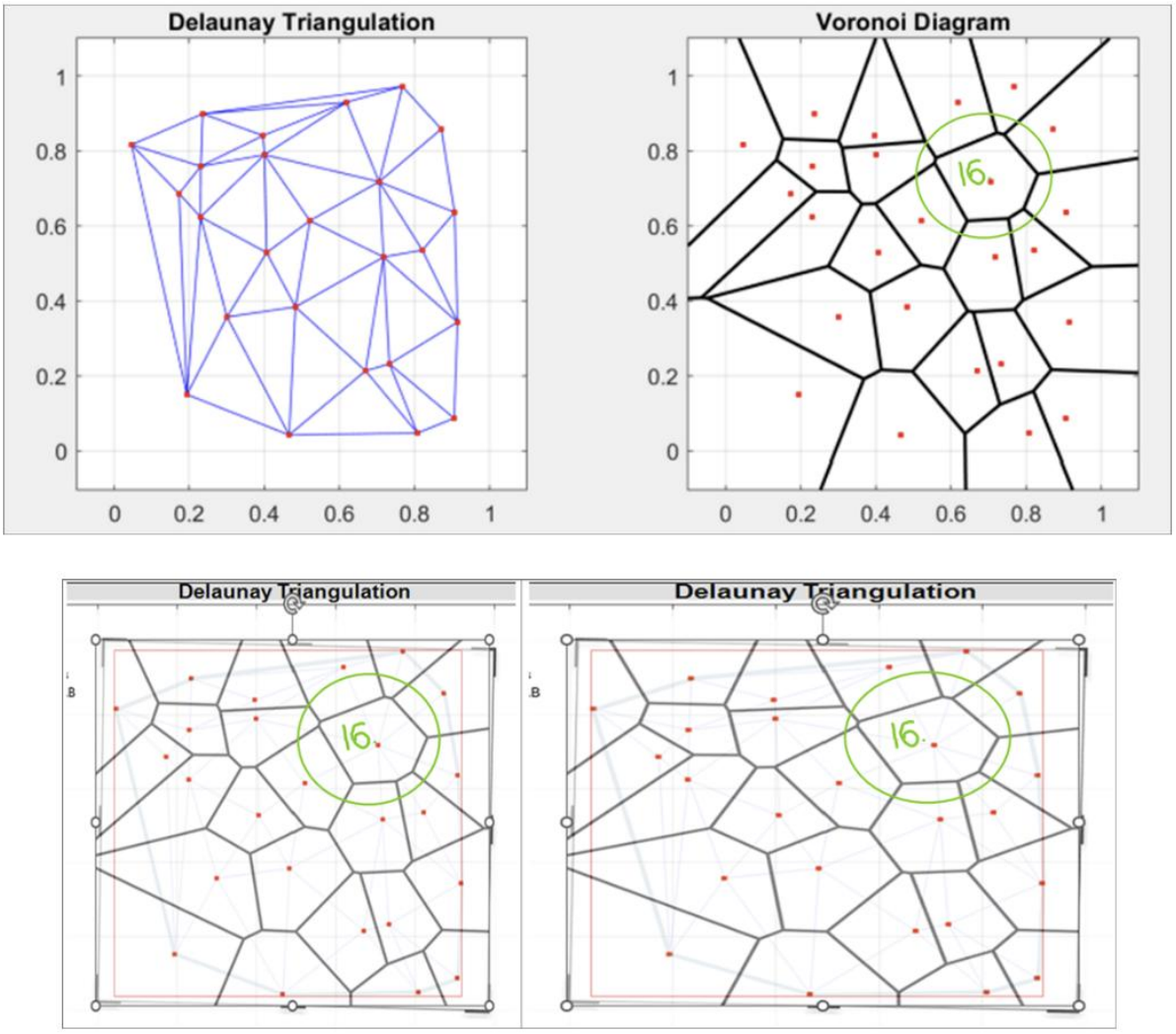

Figure 5. *Cell 16 Geometric Analysis. (Right-Top) Cell 16 highlighted in MATLAB triangulation and corresponding Voronoi tessellation showing its 8-sided geometry in the distorted configuration. (Bottom) Comparison of original and transformed representations demonstrating preservation of geometric relationships and Cell 16's role as a structural anchor.*

3.4 Statistical Validation

Finally, we performed stability tests across configurations to assess robustness. Mean cell area remained identical (0.0511). Area standard deviation remained nearly unchanged (0.0435 → 0.0434). Edge entropy varied by only 0.0032 bits. Topological entropy remained exactly constant (2.1056 bits).

Side-count distributions changed only in the disappearance of the 8-sided cell. With Cell 16: 4-sided (3), 5-sided (6), 6-sided (3), 7-sided (2), 8-sided (1). Without Cell 16: 4-sided (2), 5-sided (5), 6-sided (5), 7-sided (2).

Cross-platform reproduction yielded the same geometric, topological, and entropic properties across manual reconstruction, MATLAB, and secondary computational environments, confirming that the observed behaviors are inherent system properties rather than platform-specific artifacts.

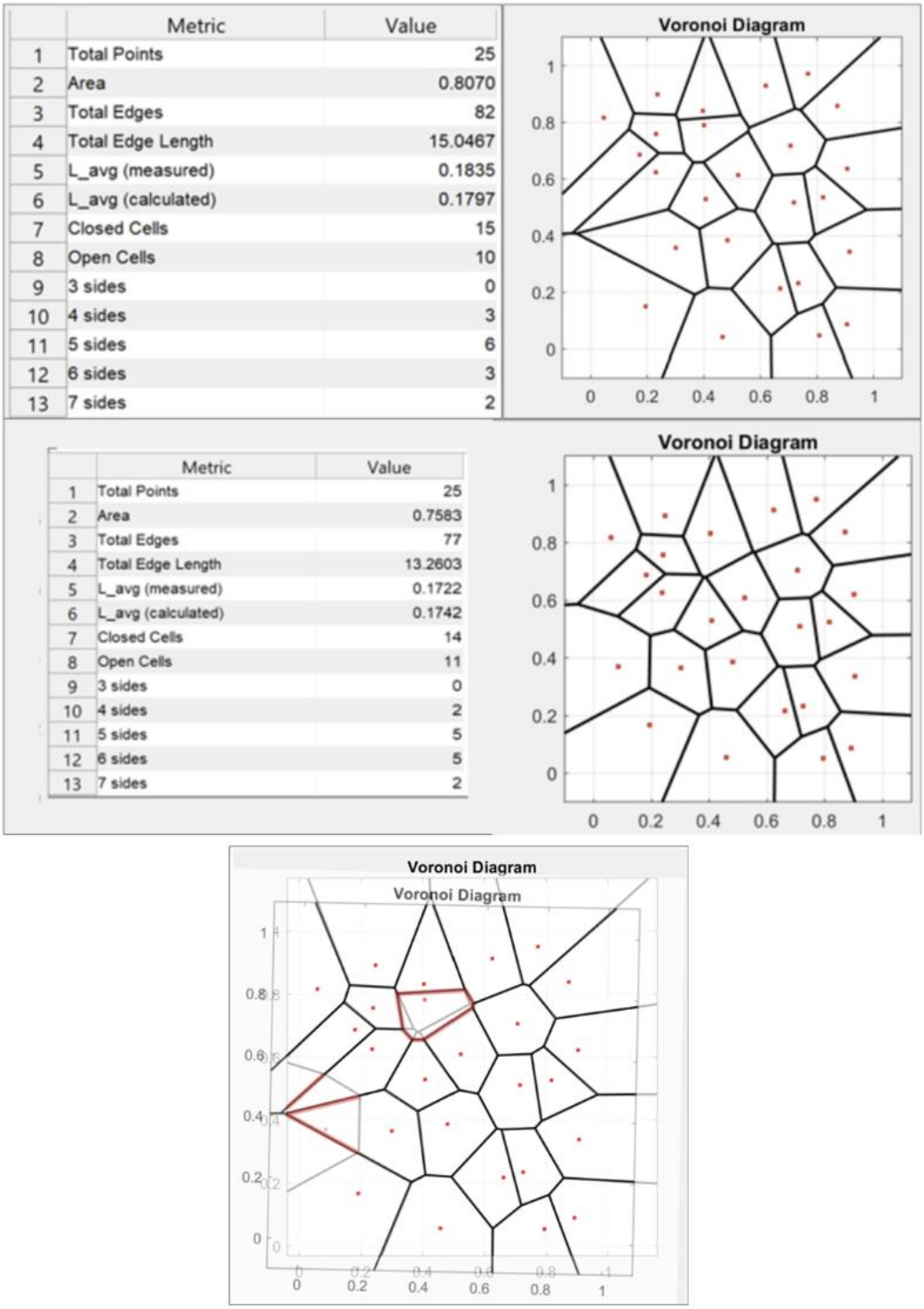

	Metric	Value
1	Total Points	25
2	Area	0.8070
3	Total Edges	82
4	Total Edge Length	15.0467
5	L_avg (measured)	0.1835
6	L_avg (calculated)	0.1797
7	Closed Cells	15
8	Open Cells	10
9	3 sides	0
10	4 sides	3
11	5 sides	6
12	6 sides	3
13	7 sides	2

	Metric	Value
1	Total Points	25
2	Area	0.7583
3	Total Edges	77
4	Total Edge Length	13.2603
5	L_avg (measured)	0.1722
6	L_avg (calculated)	0.1742
7	Closed Cells	14
8	Open Cells	11
9	3 sides	0
10	4 sides	2
11	5 sides	5
12	6 sides	5
13	7 sides	2

Figure 6. *Ghost Cell Manifestation and Information Preservation. (Top) Two Voronoi diagrams generated from the same 25 points in different configurations, with corresponding structural metrics. (Bottom) Overlapping visualization of system's information preservation mechanisms: ghost cell (pale red) demonstrates area compensation; stable region of Cell 16 (black) shows information preservation; transformed boundaries (grey) reveal systematic adaptation. Red outlines highlight critical transition regions.*

Table 5. Summary of Invariant Global Metrics

Global Metric	Value (Mean)	Std. Dev. (σ)	Status
Mean Cell Area	0.0511	—	Identical across both states
Area Std. Dev. (σarea)	—	0.0435 → 0.0434	Nearly constant
Lavg (Calculated)	≈ 0.17	—	Consistent with theoretical predictions
Unusual Tags	1 (Cell 16) → 0	—	System returns to valid state

4. Discussion

4.1 Truth Preservation via Boundary Permeability

The 25-point investigation reveals that truth preservation in Voronoi systems is governed not by local geometric precision alone, but by topological boundary permeability. The contrast between the distorted and true configurations demonstrates this mechanism clearly.

In the distorted state, the system contained 15 closed cells and 10 open cells. A single misplaced seed point produced a Voronoi cell that was artificially closed within the interior of the domain, despite its correct geometric role being boundary-interacting. This false closure trapped information that should have interacted with the domain boundary. As a consequence, topological stress accumulated in the neighboring region, forcing Cell 16 to expand into an 8-sided polygon—a configuration associated with increased entropy and structural tension.

In the true state, relocating the seed to its correct position did not merely correct a coordinate error. It changed the topological status of the ghost cell from closed to open, reconnecting it with the domain boundary. This transition restored the correct balance between closed and open regions (14 closed / 11 open cells). Once boundary permeability was restored, the excess stress on Cell 16 was released, allowing it to relax back into a 7-sided polygon.

This observation demonstrates that the system preserves truth by adjusting openness to the boundary, rather than by enforcing local uniformity. Errors manifest as states of false closure; corrections restore openness. The Voronoi system compensates for geometric distortion through topological reconfiguration, ensuring that the correct number of regions interact with the boundary.

4.2 The Inverse Bias Paradox

An unexpected but central insight emerged from the decision-making process during the investigation itself. When selecting between the two configurations, the distorted state was consciously chosen for further analysis because it appeared messier and therefore more "realistic" to the human eye. The more balanced configuration—produced by the natural physical drop of the seeds—appeared suspiciously orderly and was initially distrusted.

Quantitative analysis contradicted this intuition. The naturally formed, resting configuration exhibited lower area entropy than the human-selected distorted configuration. Specifically, the forced configuration increased entropy by approximately 0.11 bits, despite being chosen to simulate realism.

This finding exposes an *inverse bias of pessimism*: the assumption that natural systems must appear irregular, noisy, or imperfect, and that apparent balance signals artificiality. The data show the opposite. Nature optimizes for efficiency, not visual messiness. Human attempts to

"correct" or simulate natural imperfection introduce noise, increase entropy, and distort topology.

The implication is not that order is inherently natural and disorder artificial, but that externally imposed intention—whether toward order or disorder—injects entropy. The lowest entropy state is the resting state of the system, free from human correction.

4.3 Natural Chaos vs. Artificial Distortion: Digital Forensics

A critical empirical distinction emerges when examining how the system responds to different kinds of irregularity. The naturally generated configuration contained clear local clustering and uneven spatial distributions. These clusters were accepted by the computational analysis as valid geometric outcomes. None triggered anomalous topological features, and none produced cells exceeding the typical 7-sided structure.

In contrast, a single artificial displacement of one seed point produced a distinct response: the formation of an 8-sided cell marked as "unusual" by the computational system. This response was not triggered by natural randomness, density variations, or local clustering. It was triggered exclusively by forced geometric distortion.

This demonstrates that the system distinguishes between natural chaos and artificial manipulation. Natural randomness is absorbed without topological alarm. Artificial interference generates detectable structural stress.

The "unusual" tag thus functions as a form of digital immune response—a topological indicator that geometry has been pushed out of its natural equilibrium. This is not a visual judgment; the distorted configuration looked realistic to a human observer. The distinction emerges only through structural analysis.

4.4 Scale and the Minimum Necessary Bias

The clarity of these findings depends critically on scale. The 25-point system is small enough that topological effects dominate statistical averaging. In large-N systems, local distortions are diluted, anomalies blend into distributions, and bias becomes difficult to isolate.

Here, the limited scale made human bias measurable. The investigator's subjective choice directly altered the system's entropy and topology in a quantifiable way. The system's response—ghost cell formation, topological mutation, entropy increase—rendered that bias observable.

Thus, human limitation was not a flaw of the experiment but a necessary experimental condition. The small system acted as an amplifier of bias, transforming subjective choice into objective signal.

4.5 Implications for Truth-Preservation Frameworks

These findings provide a concrete empirical foundation for truth-preservation frameworks in information systems [4, 5]. The system does not detect manipulation based on visual plausibility or statistical rarity. It detects forced geometry—deviations from natural equilibrium that disrupt boundary interaction and topological balance.

This capability is directly relevant to detecting deepfakes, manipulations, and synthetic distortions. Artificial constructs can appear realistic while still violating underlying structural

constraints. The geometric approach operates at this deeper level, identifying distortion through topological stress rather than surface appearance.

Importantly, this detection operates in small, intimate systems, not only at massive data scales. The mechanism is local, structural, and representation-independent, making it suitable for applications where subtle manipulation must be identified without reliance on training data or pattern matching.

5. Conclusion

This study presents a detailed empirical investigation of a 25-point Voronoi system, revealing fundamental principles of geometric information preservation across physical, manual, and computational representations.

We identified two distinct transformation regimes governing physical-digital translation: the Digital Offset Constant ($\lambda_x \approx 0.689$) arising from computational geometry processing, and the physical-digital alignment factor (≈ 0.767) derived from skeletal perimeter analysis. We quantified stable entropy measures across configurations, with topological entropy remaining invariant (2.1056 bits) and area entropy showing a measurable 0.11-bit reduction upon correction of artificial distortion.

We documented a systematic compensation mechanism triggered by artificial distortion. The appearance and resolution of the ghost cell demonstrated that Voronoi systems preserve truth through topological boundary management, not local geometric enforcement.

Crucially, the investigation revealed that human bias—even when attempting to simulate realism—introduces measurable entropy and structural distortion. Natural resting states exhibited lower entropy than human-selected alternatives, exposing an inverse bias of pessimism embedded in intuitive judgment.

Finally, the system's ability to distinguish natural randomness from artificial manipulation establishes a basis for topology-driven digital forensics. These findings support broader frameworks for truth preservation in information systems and suggest that small-scale geometric systems can function as sensitive detectors of forced structure and informational falsification.

5.1 Future Work

Several directions emerge from this work. Extended analysis of larger point sets would test the scalability of compensation mechanisms. Application to real-world digital forensics scenarios would validate practical utility. Theoretical connections to hyperuniformity and information-theoretic measures warrant formal development.

Future research will examine how these entropy scaling factors align with universal geometric constants, specifically regarding the Root Protocol's scaling laws [5]. Preliminary analysis suggests these scaling factors align with geometric primitives, such as the behavior of a rhombus inscribed within a square grid. Future work will formalize this connection within the Root Protocol framework.

References

[1] Aurenhammer, F., Klein, R., & Lee, D.-T. (2013). *Voronoi Diagrams and Delaunay Triangulations*. World Scientific Publishing. https://doi.org/10.1142/8685

[2] Bormashenko, E., Frenkel, M., Vilk, A., Legchenkova, I., Fedorets, A. A., Aktaev, N. E., Dombrovsky, L. A., & Nosonovsky, M. (2018). Characterization of self-assembled 2D patterns with Voronoi entropy. *Entropy*, 20(12), 956. https://doi.org/10.3390/e20120956

[3] Shannon, C. E. (1948). A mathematical theory of communication. *Bell System Technical Journal*, 27(3), 379–423. https://doi.org/10.1002/j.1538-7305.1948.tb01338.x

[4] Keynan, M. (2025). *TROOT: Entropy-Calibrated Symbolic Language System for Truth Preservation and Information Ordering*. U.S. Provisional Patent Application No. 63/928,912, filed December 2, 2025.

[5] Keynan, M. (2025). *The Root Protocol: Systems, Methods, and Geometric Protocols for Universal Scaling, Data Preservation, and Entropic Optimization*. U.S. Provisional Patent Application No. 63/934,646, filed December 9, 2025.

Acknowledgments

The author acknowledges the value of independent, empirically-grounded investigation in uncovering fundamental geometric principles. Computational analysis was performed using MATLAB. This work was conducted as part of an independent research initiative.

Appendix: Data Availability

Original physical photographs, coordinate data, MATLAB scripts, and detailed measurement logs are available upon reasonable request from the author. Replication protocols follow standard procedures for Voronoi tessellation construction and analysis.